Solar Energy Materials & Solar Cells 208 (2020) 110352

Contents lists available at ScienceDirect

Solar Energy Materials and Solar Cells

journal homepage: http://www.elsevier.com/locate/solmat

High-efficiency perovskite solar cell using cobalt doped nickel oxide hole transport layer fabricated by NIR process

Pei-Huan Lee [a], Bo-Ting Li [a], Chia-Feng Lee [b], Zhi-Hao Huang [b], Yu-Ching Huang [b,*], Wei-Fang Su [a,**]

[a] Dept. of Materials Science and Engineering, National Taiwan University, Taipei, Taiwan
[b] Dept. of Materials Engineering, Ming Chi University of Technology, New Taipei, Taiwan

ARTICLE INFO

Keywords:
Perovskite solar cell
Near infrared radiation
Rapid thermal annealing
Hole transport layer
Cobalt doped nickel oxide
Interface engineering

ABSTRACT

Lead halide perovskite solar cells (PVSCs) have potential toward commercialization because of their high efficiency and low cost. The hole transport layer (HTL) of p-i-n perovskite solar cell is usually made of NiO_X. However, the NiO_X needs to be processed at 300 °C for 15 min for good hole transport property. This long heating time prohibits the development of continuous commercial process. Thus, a rapid heating process for the NiO_X film deposition is critical to realize the commercialization of PVSCs in the future. In this study, we develop a facile method to obtain high quality NiO_X films annealed by NIR in a short time of 50 s. A short-wave NIR lamp at 2500 K was used to systematically investigate the effect of NIR intensity on the film quality of sol-gel NiO_X. The PVSCs fabricated from NIR-annealed NiO_X (NIR-NiO_X) film show a comparable power conversion efficiency (PCE) to those fabricated from traditional hot-plate annealed-NiO_X (HP-NiO_X). In addition, the NIR annealed cobalt-doped NiO_X (NIR-Co:NiO_X) was synthesized to replace pristine NIR-NiO_X. The PCE of PVSCs fabricated from this new NiO_X film can be increased from 15.99% to 17.77%, which is due to the efficient hole extraction, less charge accumulation, and reducing V_{oc} loss resulting from the improved hole mobility, reduced interface resistance and well-matched work function. Our study paves a way to fulfill the requirements of low cost and low energy consumption of large scale production of high efficiency PVSCs.

1. Introduction

Organic-inorganic metal halide perovskites are well-known material for their excellent optical [1], tunable electronic [2–4] and solution processable properties. Owing to these excellent properties, organic-inorganic metal halide perovskite materials have been used to fabricate low cost and high efficiency solar cells (PVSCs) in recent years [5]. To date, a certified high power conversion efficiency (PCE) of 24.2% has been achieved [6]. Except the need for good quality of perovskite film [7-8], the quality of electron and hole transport layers (ETL and HTL) are also important for high performance PVSC [9]. The perovskite layer is sandwiched between these two layers which significantly affect the charge transport behavior, interfacial charge accumulation, and energy loss of photogenerated carriers [10–13]. The PVSCs with planar p-i-n structure are attracting great attention because they are less hysteresis, simple architecture and using low temperature and cost-effective fabrication process. For the planar p-i-n structure PVSCs, many p-type materials including organic and inorganic materials, such as PEDOT:PSS [14–16], PTAA [17–19], MoO_3 [20], CuSCN [21–24], CuO_X [25,26] and NiO_X [12,27,28], have been utilized as potential HTL. The HTL is located between transparent electrode and perovskite layer. Among those materials, nickel oxide (NiO_X) has become a material of choice as the HTL of the p-i-n PVSC due to its good chemical stability, high optical transmittance and deep-lying valence band [12].

Many deposition techniques of NiO_X thin films have been developed, including solution process [27–36], sputtering [37–39] and atomic layer deposition [40]. Among these techniques, the solution process draws the most attention due to its low manufacturing cost and the feasibility for large scale process. The sol-gel solution process is usually adapted to fabricate NiO_X film, but it requires high reaction temperature (>300 °C) and long heating time (>15 min) to form a high crystalline film, which is a high energy consumption and a barrier for continuous commercial

* Corresponding author.
** Corresponding author.
E-mail addresses: huangyc@mail.mcut.edu.tw (Y.-C. Huang), suwf@ntu.edu.tw (W.-F. Su).

https://doi.org/10.1016/j.solmat.2019.110352
Received 24 July 2019; Received in revised form 17 November 2019; Accepted 8 December 2019
Available online 26 December 2019

process and fabricating flexible PVSCs. Although, a lot of strategies have been developed for depositing the NiO_X thin films at low temperature (<150 °C), such as combustion method [41,42] and hydroxide assisted energy conservation method [43], all these methods still need the long heating time of more than 30 min.

Recently, near-infrared (NIR) radiation method has been explored as a quick heat approach to process metals, metal oxides and perovskite films. Hooper et al. used NIR radiation method to sinter TiO_2 film for dye sensitized solar cell in just 12.5 s [44]. Baker et al. used NIR radiation method to heat m-ZrO_2 and m-carbon, and the processing time was greatly reduced from over 2 h to less than 25 s [45]. The NIR radiation method has also been used to heat perovskite layer of PVSCs [46–49]. Troughton et al. used NIR radiation to anneal $MAPbI_3$ in 2.5 s with a PCE of 10.0% compared to 10.9% for a 45 min oven-annealed devices [46]. Pool et al. reduced the annealing time of $FAPbI_3$ from 10 min to 40 s by NIR radiation method [47]. Therefore, NIR radiation method is an effective way to shorten processing time.

However, the PCE of PVSC fabricated from NiO_X is relatively low because of the low conductivity of NiO_X. The low conductivity of HTL would reduce hole extraction efficiency and cause the interfacial charge accumulation. Doping other metal atoms has been proven an effective way to improve the conductivity of metal oxide. For NiO_X, metal dopants, such as Li [35], Cu [29,30,50], Cs [31,36], Co [32,37], Ag [33], and Sr [34] are usually used. In addition to the conductivity, the work functions of doped-NiO_X are also varied with dopants, and the work function of NiO_X is important for the V_{oc} of PVSC. For example, Li:NiO_X showed a undesirable positive shift of work function and that causes a reduction of the V_{oc} [35]. The dopants of Cu, Cs or Ag can deeper the work function level of NiO_X and enhance the built-in potential of PVSCs which result in the less charge accumulation, low V_{oc} loss, and PCE improvement of PVSCs. Therefore, finding a suitable metal dopant for NiO_X is critical for p-i-n PVSCs.

In this study, we develop a facile method to obtain high quality NiO_X films annealed by NIR in a short time. We used a short-wave NIR lamp at 2500 K as the heating source to anneal sol-gel NiO_X films, and systematically investigated the effect of NIR intensity on the quality of sol-gel NiO_X films. The PVSCs fabricated from the NIR-annealed NiO_X (NIR-NiO_X) film show a comparable PCE to those fabricated from the traditional hot-plate annealed-NiO_X (HP-NiO_X). In addition, the NIR-NiO_X film is replaced by NIR annealed cobalt-doped NiO_X (NIR-Co:NiO_X) film to further improve the PCE of PVSCs from 15.99% to 17.77%. The result is due to the less charge accumulation, and decreasing V_{oc} loss causing by the improvement of hole mobility, the reduction of interface resistance and well-matched work function. We successful developed a highly-efficient PVSCs fabricated from the Co-doped NiO_X HTLs by using a quick annealing NIR radiation process. Our study paves a way to fulfill the requirements of low cost and low energy consumption of large scale production process for high efficiency PVSCs.

2. Experimental method

2.1. Preparation of NiO_X and Co:NiO_X films

Two annealing methods, hot-plate and NIR radiation, were used to fabricate NiO_X films. FTO coated glass substrates (7 Ω, FrontMaterials Co. Ltd.) were cleaned sequentially with ammonia, hydrogen peroxide, deionized water, methanol and isopropanol then treated with oxygen plasma for 15 min. The 0.5 M NiO_X precursor solution was prepared by mixing nickel acetate tetrahydrate (Sigma-Aldrich, 98%) and 1 molar equivalent of ethanolamine (Sigma-Aldrich, 99%) in ethanol. The 0.5 M Co:NiO_X precursor solution was prepared by replacing nickel acetate tetrahydrate to cobalt acetate tetrahydrate (Sigma-Aldrich, 98%) of 2, 4, 8 mol% in a mixture of ethanol and deionized water(in 95:5 vol ratio). Both of solutions were stirred till acetates entirely dissolved and filtered by 0.22 μm PTFE filter. Then, either NiO_X or Co:NiO_X precursor solution was spin-coated on cleaned FTO glass at 4000 rpm for 20 s. For the preparation of hot-plate annealed NiO_X films, the NiO_X precursor films were subsequently annealed on hot-plate at 300 °C for different time. The NIR equipment (Taiti Technology Co. Ltd. Taiwan) containing halogen short-wave NIR lamps at 2500 K with the power density of 125 kW/m^2 (at peak of ~1100 nm) was selected to prepare NIR annealed NiO_X or Co:NiO_X films. The distance between lamp and sample was maintained at 5 cm. Note that all of the samples were prepared in the air.

2.2. Fabrication of PVSCs

The 1.2 M perovskite precursor solution was prepared by mixing MAI (FrontMaterials Co. Ltd.) and PbI_2 (FrontMaterials Co. Ltd.) (in 1:1 M ratio) in 1 mL mixed solvent of *N,N*-dimethylformamide (Sigma-Aldrich, 99.8%) and dimethyl sulfoxide (Sigma-Aldrich, 99.8%) (in 5:2 vol ratio). The perovskite film was prepared by spin coating the precursor solution onto the as-prepared NiO_X or Co:NiO_X film coated FTO substrate (FrontMaterials Co. Ltd.) at 4500 rpm for 30 s in a glove box. At the 15 s of the spinning process, a 300 μL of diethyl ether was dropped onto the coated sample to wash out the extra solvent and form transparent intermediate phase of perovskite. Then, all of the samples were sequentially annealed on hot-plate at 70 °C for 1 min and 100 °C for 2 min to form dark-brown perovskite films. Afterward, the [6,6]-phenyl-C61-butyric acid methyl ester ($PC_{61}BM$, FrontMaterials Co. Ltd.) solution (2.5 wt% in chlorobenzene) was spin-coated onto perovskite layer at 1000 rpm for 30 s to serve as the electron transporting layer. Finally, the work function modifier polyethylenimine (PEI, 0.1 wt% in isopropanol) was spin-coated onto the $PC_{61}BM$ layer, followed by 100 nm Ag electrode deposited by thermal evaporation. The device architecture of planar p-i-n PVSCs is FTO/NIR-NiO_X or NIR-Co:NiO_X/$MAPbI_3$/$PC_{61}BM$/PEI/Ag, as shown in Fig. 1a Fig. 1b illustrates the band diagram of each layer of PVSCs. The energy levels of FTO, $MAPbI_3$, $PC_{61}PM$ and Ag were obtained from literature [30,36], and the work function of NIR-NiO_X and NIR-Co:NiO_X were measured by ultraviolet photoelectron spectroscopy.

2.3. Characterization of devices

The J-V curves of devices were measured by a voltage source meter (Keithley 2410) under an AM 1.5G solar simulator (Enli Tech, SS-X100R) with an irradiation of 100 $mWcm^{-2}$. Note that all of the devices were not encapsulated and all the measurement were performed in air with 40% RH. The work function of NiO_X and Co:NiO_X films were measured by ultraviolet photoelectron spectroscopy (PHI 5000 VersaProbe, ULVAC-PHI) using ultraviolet light source of He I emission (21.2 Ev, B50 W) and calculated by the equation of $\Phi = h\nu - (E_0 - E_F)$. The crystal structures of annealed NiO_X films either by hot plate or NIR were determined by X-ray diffraction spectrometry (XRD) (Rigaku, TTRAXIII, Japan) using Cu Kα radiation at 18 kV. The X-ray diffraction of NIR-NiO_X and NIR-Co:NiO_X were measured at the 23 A beamline of the National Synchrotron Radiation Research Center (NSRRC), Taiwan. The X-ray photoelectron spectroscopy (XPS) spectra were recorded with a PHI 5000 Versa Probe system (ULVAC-PHI, Chigasaki) using a micro focused (100 μm, 25 W) AI X-ray beam. The surface morphology and height information of NiO_X and Co:NiO_X films were measured by atomic force microscopy (AFM, OMV-NTSC, Bruker). The UV–visible transmittance spectra were obtained by UV–vis spectrometer (V-730, Jasco). The PL spectra were recorded with a continuous-wave diode laser source (PDLH-440-25, DongWoo Optron Co. Ltd.), and the emission spectra were recorded with a photomultiplier tube detector system (PDS-1, DongWoo Optron Co. Ltd.). The TRPL spectra were recorded using a time correlated single photon counting spectrometer (WELLS-001, FX, DongWoo Optron Co.Ltd.). The pulse laser had a wavelength of 440 nm and an average power of 1 mW was operated with excitation duration of 2 μs. To figure out the resistive and capacitive properties of NiO_X/perovskite interface, devices were fabricated with FTO/NiO_X/perovskite/Au structure. The measurement was carried out in ambient

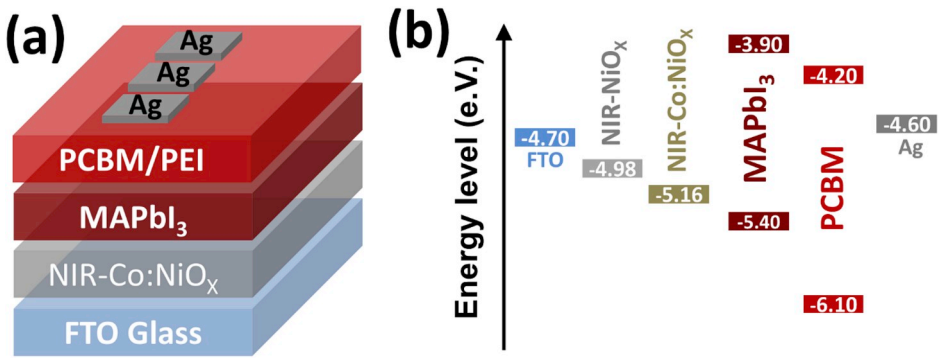

Fig. 1. (a) Device structure and (b) energy band diagram of planar p-i-n perovskite solar cell.

condition with 1 sun illumination (AM1.5G, 1 kW/m^2). The AC perturbation was 10 mV while the devices were working at open-circuit condition. The impedance spectra were recorded in the frequency range from 100 mHz to 1 mHz with a Zahner IM6eX electrochemical workstation.

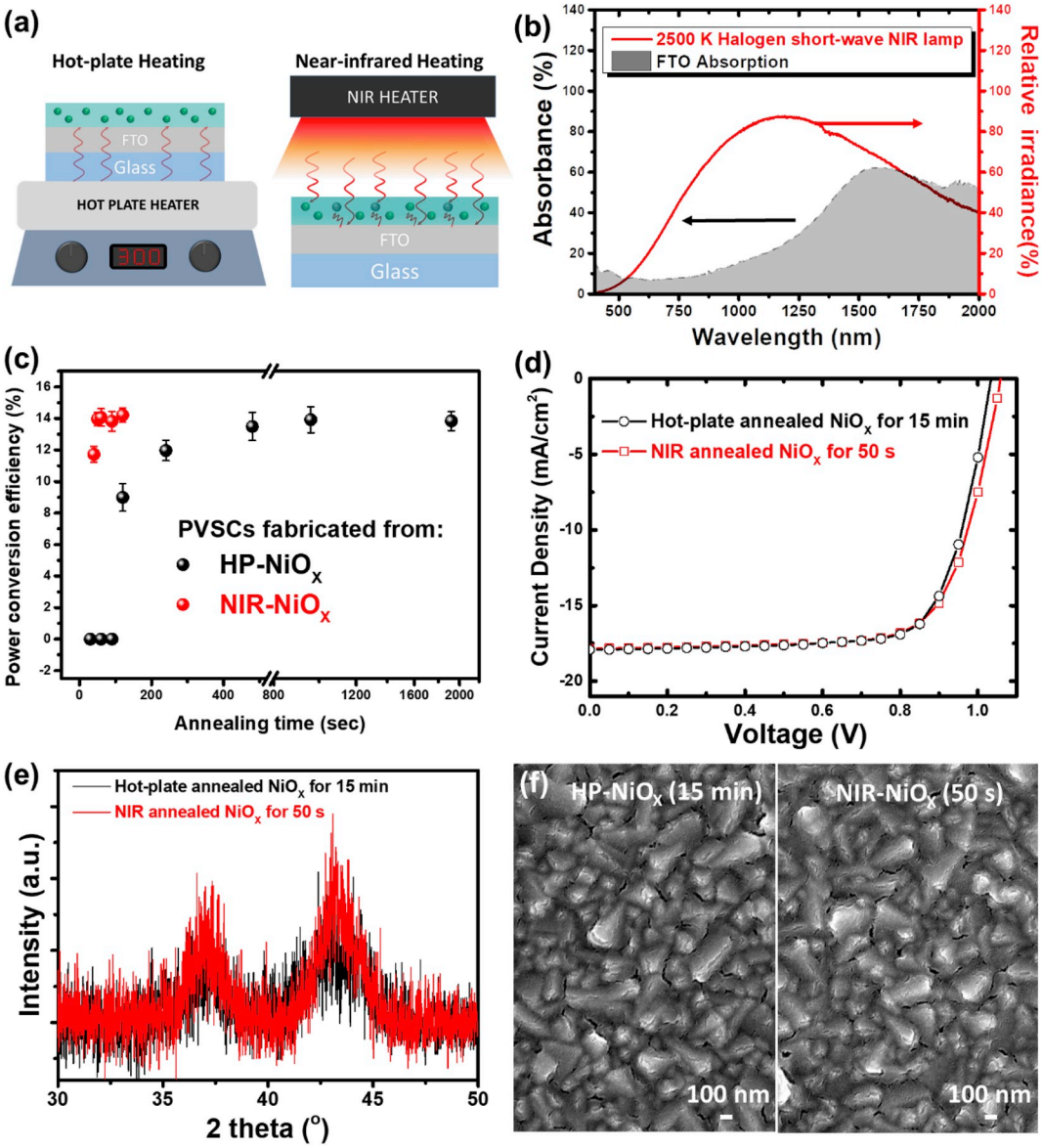

Fig. 2. **(a)** Schematic processing diagrams of hot-plate and NIR heating method. **(b)** Absorption spectrum of FTO glass and irradiance spectrum of short-wave NIR lamp with 2500 K. **(c)** Performance variation of PVSCs fabricated from hot plate and NIR annealed NiO_X HTL with different annealing time. **(d)** J-V curves of the PVSCs fabricated from hot plate and NIR annealed NiO_X HTL. **(e)** Crystallinity and **(f)** surface morphology of the two NiOx films.

3. Results and discussion

In order to obtain high quality NiO_X film using short annealing time, we introduced the NIR radiation technique to anneal NiO_X film, and compared with the film quality annealed by conventional hot-plate heating method. Fig. 2a shows the schematic diagrams of two annealing processes for a sample of NiO_X on FTO (NiO_X/FTO). Fig. 2b shows the UV–Vis–NIR absorption spectrum of FTO substrate and the relative irradiance of the halogen NIR lamp at 2500 K. The FTO contains large amount of free carriers which can absorb NIR photons and then generates much heat. The highly overlapping region indicates that many NIR photons can be absorbed by the FTO substrate. Thus, upon NIR exposure, the NIR photons are immediately absorbed by FTO as heat source to anneal NiO_X less than 1 min. On the contrary, the hot plate process, the heating is through gradual thermal conduction FTO first, then slow heat transfer to anneal NiO_X. Therefore, the extend period of time such as 15 min or longer is required to anneal NiO_X/FTO with sufficient crystallinity. To elucidate the quality of NiO_X film annealed by NIR radiation (NIR-NiO_X) and hot-plate (HP-NiO_X), we deposited the NiO_X films with various annealing times, and then observed the PCE variations of the PVSCs using these NiO_X films as HTL. At first, we fabricated PVSCs with devices structure of FTO/NIR-NiO_X or HP-NiO_X/$MAPbI_3$/$PC_{61}BM$/PEI/Ag to evaluate the performance of PVSCs. The NIR-NiO_X or HP-NiO_X were serve as HTL. The perovskite ($MAPbI_3$) films were fabricated by solvent engineering method with the dropping of diethyl ether during the spinning process. The electron transporting layer, $PC_{61}BM$, was followed by the PEI work function modifier, which can reduce the barrier between $PC_{61}BM$ and Ag electrode for extracting electron effectively. Fig. 2c shows the change of PCE of PVSCs fabricated from NiO_X film annealed either by NIR or hot-plate with various annealing times. The detailed NIR-NiO_X optimization results are illustrated in the supporting information (Fig. S1). The PCE of PVSCs fabricated from HP-NiO_X can be increased with increasing anneal time of HP-NiO_X and reached a plateau of 14% as the HP-NiO_X was annealed with enough time (>900 s). This result implies that the film quality of HP-NiO_X is highly dependent on the annealing time, and the insufficient annealing time for HP-NiO_X film would result in a poor PCE of PVSCs. As for PVSCs fabricated from NIR-NiO_X, the devices can reach a comparable PCE to PVSCs fabricated from HP-NiO_X at the annealing time less than 1 min. Fig. 2d shows the J-V curves of PVSCs fabricated from HP-NiO_X and NIR-NiO_X films, and the two devices almost exhibit a similar J_{sc}, V_{oc} and FF at optimized process condition, which indicate that the NIR process is an effective way to shorten the annealing time of NiO_X. To further clarify the film quality of HP-NiO_X and NIR-NiO_X films, we examined the crystallinity and morphology of the two films by using x-ray diffraction (XRD) and scanning electron microscope (SEM). Fig. 2e shows the NiO_X film exhibits two main peaks at 2 theta = 37.8° and 43.7°, representing (111) and (200) crystal planes of rock salt NiO, respectively. The NIR-NiO_X film with 50 s annealing time shows a higher crystallinity than that of HP-NiO_X with 15 min annealing time, indicating that the NIR annealing method is able to form NiO_X film with sufficient crystallinity in a short time. The SEM images of HP-NiO_X with 15 min annealing time and NIR-NiO_X films with 50 s annealing time are shown in Fig. 2f. The results show that the morphology of the NiO_X film annealed by the rapid annealing method is same as the films annealed by hot-plate. Although NIR-NiO_X films are formed in a very short time, it is still dense and free of voids. According to these results, we can suggest that the incomplete crystallization of NiO_X film is the main reason for the low PCE of PVSCs. It is noteworthy that the crystallinity of NIR-NiO_X film is increased with increasing annealing time and NIR power (Fig. S2). Generally speaking, the higher crystallinity of NiO_X is good for the charge transfer and PCE improvement. However, our results are not fully consistent with this statement. We explain that by analyzing the photovoltaic characteristics and the surface morphology. Fig. S3 and Table S1 summarize the performances of PVSCs fabricated from 100% NIR-NiO_X with various annealing time (60 s, 90 s and 120 s). From the XRD results, we know that the longer annealing time, the higher crystallinity of NIR-NiO_X films. Fig. S3 illustrates that the increasing current density with the raising annealing time, and we can attribute the increasing current density to the enhancing crystallinity of NIR-NiO_X films. In contrast to current density, the V_{oc} and FF are declined with the raising annealing time. We proposed the decreasing V_{oc} and FF result from the evolution of surface morphology of NIR-NiO_X films. Fig. S4 shows the high-resolution SEM images of the NIR-NiO_X films under various irradiation power for different time, and we can see that the NiO_X films form more cracks with the increasing NIR annealing time. The cracks in the NiO_X films would become charge traps and retard the charge transport, resulting in the V_{oc} loss and low FF of PVSCs. These results reveal a trade-off between crystallinity and surface morphology, therefore, the PCEs of PVSCs with NIR annealing for 50 s and 120 s are similar. Consequently, to reduce the processing time of NiO_X films, we use the 100% power NIR radiation for 50 s as annealing method for the following study.

To further improve the efficiency of the PVSCs using NIR-NiO_X as HTL, we doped cobalt into NiO_X (Co:NiO_X) with different concentration (0, 2, 4 and 8 mol. %). The cross-section SEM image (Fig. 3a) shows each layer of the device including NIR-Co:NiO_X, $MAPbI_3$ and $PC_{61}BM$/PEI with thickness of 80, 375 and 60 nm, respectively. The photovoltaic characterizations and J-V curves of the devices with different doping concentration are summarized in Table 1 and shown in Fig. 3b The average PCE of PVSCs fabricated from pristine NIR-NiO_X film is 15.35%, with V_{oc} of 1.06 V, J_{sc} of 18.52 mA/cm^2, and FF of 78.53%. The effect of Co doping on the PCE of PVSCs is clear, the average PCE can be improved to 15.81 and 16.26% for a Co-doping concentration of 2 (NIR-2 Co:NiO_X) and 4 mol%, (NIR-4 Co:NiO_X) respectively. The increasing PCE of PVSCs with NIR-Co:NiO_X mainly results from the J_{sc} improvement. As the Co-doping concentration further increases to 8 mol% (NIR-8 Co:NiO_X), the PCE of PVSCs is decreased to 13.61% resulting from the J_{sc} and FF reduction. Therefore, we chose the PVSCs fabricated from the NIR-4 Co:NiO_X to further hysteresis study. Fig. S5 shows J-V curve of forward-reverse scan, steady photocurrent and stabilized PCE, which confirms the negligible hysteresis of our devices. Moreover, we also illustrates the variation of photovoltaics characterizations of the PVSCs fabricated from different Co-doping concentration NiO_X films in Fig. 3c and d, and the PVSCs with NIR-4 Co:NiO_X performed a good reproducibility. To understand the improvement of device performance using NIR-4 Co:NiO_X HTL, we carried out the detailed analysis of crystallinity, morphology, work function, surface chemistry, photoluminescence, conductivity and impedance of the devices with NIR-NiO_X film or NIR-4 Co:NiO_X.

The crystal structure and film morphology of the NIR-NiO_X and NIR-4 Co:NiO_X films by XRD and atomic force microscopy (AFM), respectively. We used the synchrotron light with the wavelength of 0.1 nm to obtain the X-ray diffraction pattern. The pristine NiO_X is commonly known as the rock salt structure with octahedral site Ni^{2+} and O^{2-}. Fig. 4a shows that the pristine NiO_X exhibits the diffraction peak of (111) and (200) planes located at 2 theta of 24.5° and 28.5°, respectively. The NIR-4 Co:NiO_X shows less lattice distortion and non-shifted diffraction peak of (111) and (200) planes. Fig. 4b and c show the AFM surface morphologies of NIR-NiO_X and NIR-4 Co:NiO_X respectively. Both NiO_X and Co-doped NiO_X films are uniform and pinhole-free, and there are no significant differences in the two films. The surface root mean square (RMS) of NIR-NiO_X and NIR-4 Co:NiO_X are 20.0 nm and 18.9 nm, respectively. Thus, the improvement of PCE should be attributed to the improving interfacial behavior between the NIR-Co:NiO_X film and perovskite layer rather than the crystalline and morphology of the HTL. The X-ray photoelectron spectroscopy (XPS) were used to study the effect of Co dopant on the NiO_X films. Fig. 5a shows the XPS spectrum of the Ni $2p_{3/2}$ peaks for NIR-NiO_X and NIR-4 Co:NiO_X films, and the results clearly show the two peaks located at 855.2 eV and 853.3 eV corresponding to Ni^{3+} and Ni^{2+}, respectively. Fig. 5b shows the XPS spectrum of the Co $2p_{3/2}$, and only the NIR-4 Co:NiO_X film exhibits a peak of Co^{2+} located at 779.8 eV. The content of Co in NIR-4 Co:NiO_X film can be

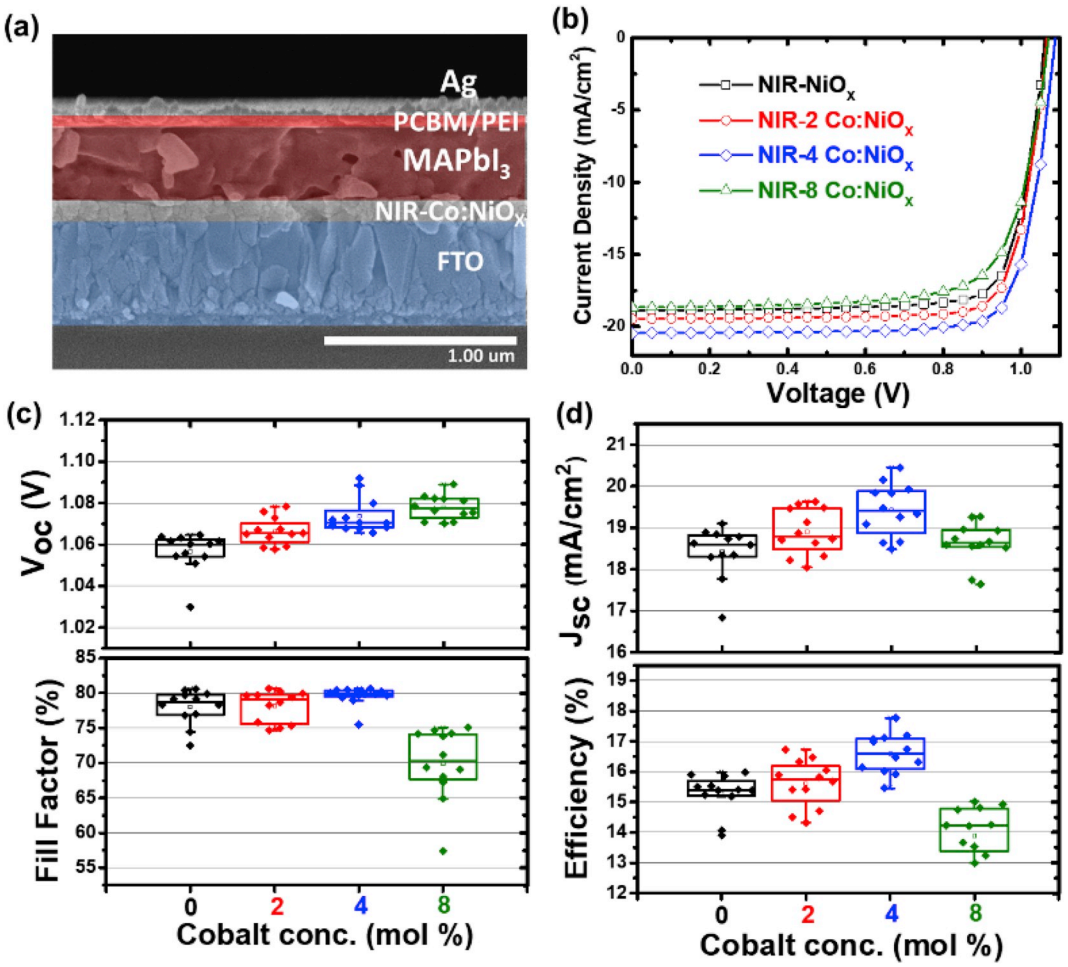

Fig. 3. **(a)** SEM cross-sectional image of planar p-i-n PVSK. **(b)** Representative J-V curves of the PVSKs with different Co doping concentration. **(c,d)** Comparison of photovoltaic characteristics of planar PVSKs fabricated from NiOx films doped with different Co concentration.

Table 1
Characteristics of planar p-i-n PVSCs fabricated from NIR-NiOx films doped with different Co concentration.

Co concentration [mol%]	V_{oc} [V]	J_{sc} [mA/cm^2]	FF [%]	Efficiency [%]
0	1.06±0.01 (1.06)	18.52±0.34 (18.89)	78.53±1.93 (79.85)	15.35±0.52 (15.99)
2	1.06±0.01 (1.07)	18.90±0.55 (19.63)	78.60±2.11 (78.65)	15.81±0.68 (16.48)
4	1.07±0.01 (1.09)	19.20±0.54 (20.46)	79.03±2.04 (79.80)	16.26±0.55 (17.77)
8	1.08±0.01 (1.07)	18.74±0.49 (18.67)	67.35±4.73 (74.15)	13.61±1.15 (14.82)

calculated ~5.1%, indicating that the Co is successfully doped into the NiO_X film. To further confirm the existence of Co, the XPS results of O 1s spectrum of NIR-NiO_X and NIR-4 Co:NiO_X are shown in Fig. 5c. The NIR-NiO_X film presents two peaks located at 528.29 and 530.05 eV, which ascribes to lattice oxygen and oxygen vacancy, respectively. Generally, chemical impurity usually induces XPS peak shift [51]. For our case, the NIR-4 Co:NiO_X film shows a binding energy shift toward high energy direction, indicating that the successfully incorporation of Co. Moreover, the more Ni^{3+} ions can induce the formation of extra holes and thus increase the conductivity of NiO_X [52]. The conductivity of NiO_X strongly relies on the microstructural defects, such as Ni^{2+} vacancies and interstitial oxygen in NiO_X crystallites [53]. The formation of Ni^{3+} ions is highly correlated with the Ni^{2+} vacancies and interstitial oxygen, therefore, previous literature indicated that the resistivity can be lowered by an increase of Ni^{3+} ion concentration [54]. Therefore, the higher Ni^{3+}/Ni^{2+} ratio is referring to the higher hole conductivity. The calculated Ni^{3+}/Ni^{2+} ratios of NIR-NiO_X and NIR-4 Co:NiO_X films are 1.54 and 1.32, respectively, indicating that the conductivity of NIR-4 Co:NiO_X might be lowered. We also measured the work function (WF) of NIR-NiO_X and NIR-4 Co:NiO_X by ultraviolet photo-electron spectroscopy (UPS). As shown in Fig. 5d, the work function of NIR-4 Co:NiO_X was shifted to −5.16 eV from the −4.98 eV of NIR-NiO_X, and the valence band remained at the same level. It is worth to note that the WF function of HTL determines the build-in potential in the devices. The high build-in potential reduces the charge accumulation at the interface between HTL and perovskite layer, and thus reduces the V_{oc} loss. Therefore, we speculate that the improvement of PCE is due to the desirable work function matching and less charge accumulation at the interface of perovskite/NIR-4 Co:NiO_X.

To investigate the conductivity of NIR-NiO_X and NIR-4 Co:NiO_X, the I–V curves were measured by hole only devices with the structure of FTO/NIR-NiO_X or NIR-4 Co:NiO_X/Ag, as shown in Fig. S6. The I–V curve demonstrates that the vertical current was decreased after replacing NIR-NiO_X with NIR-4 Co:NiO_X, representing the low conductivity of NIR-4 Co:NiO_X. Moreover, the low conductivity of NIR-4 Co:NiO_X was further demonstrated by four-point probe measurement. The resistivity of NIR-4 Co-NiO_X was increased to 5.08 kΩm from 1.66 kΩm of NIR-NiO_X. Both results are consistent with the prediction from the XPS measurement. While, the mobility of HTL is also a critical influencing

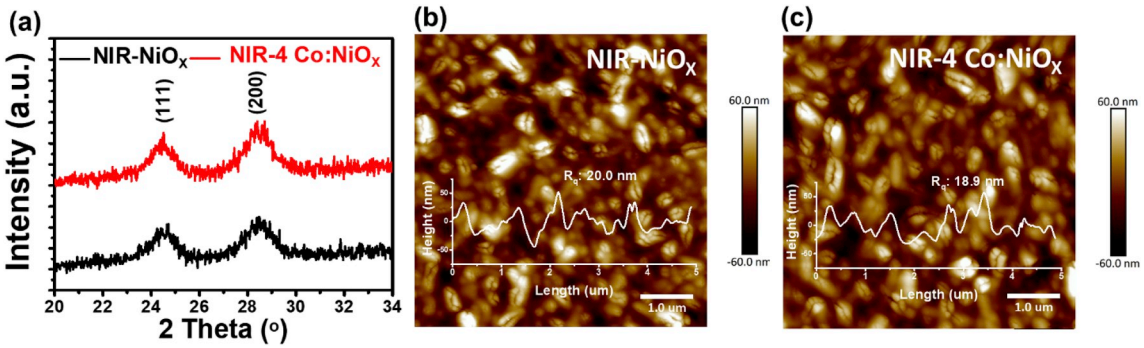

Fig. 4. Characterization of NIR-NiO_X and NIR-4 Co:NiO_X film, **(a)** XRD patterns, and **(b),(c)** AFM image and roughness.

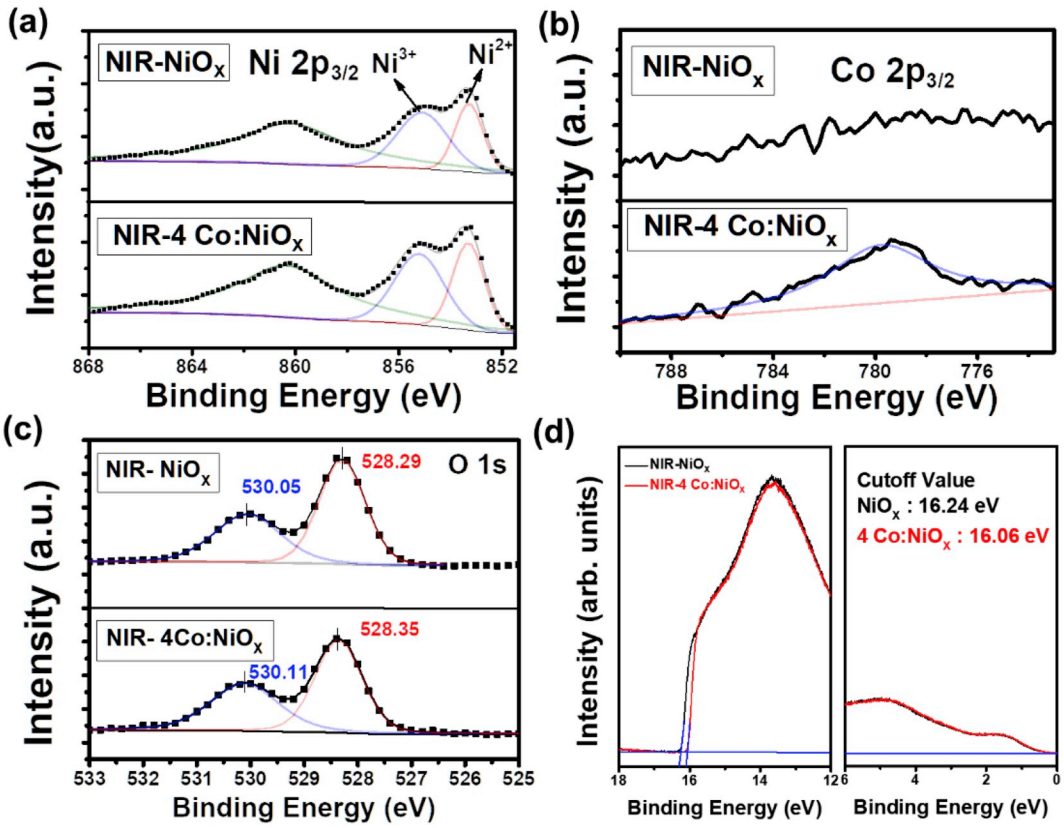

Fig. 5. XPS spectra of **(a)** Ni 2p, **(b)** Co 2p and **(c)** O 1s from NIR-NiO_X and NIR-4 Co:NiO_X films. **(d)** UPS spectra from NIR-NiO_X and NIR-4 Co:NiO_X films.

factor in the PCEs of PVSCs in addition to the conductivity of HTL. To obtain the hole mobilities of NIR-NiO_X and NIR-4 Co:NiO_X films, we use space charge limited current (SCLC) model to calculate the mobility by using hole only devices with the structure of FTO/HTL/perovskite/Au. The fitting curves are shown in Fig. 6a, and the calculated hole mobilities of NIR-NiO_X and NIR-4 Co:NiO_X films are 0.12 and 0.21 cm^2/V, respectively. The increase in hole mobility of the NIR-4 Co:NiO_X film may be resulted from that the incorporated Co^{2+} compensates the Ni^{2+} vacancy and thus reduces the ionized impurity scattering. It is provided a direct evidence that the NIR-4 Co:NiO_X film can reduce the charge recombination and enhance hole extraction rate because of the high hole mobility.

It's known that a good HTL can accelerate the charge transfer and suppress the non-radiative recombination. To investigate the charge transfer behavior at the interface of perovskite/HTL, we conducted the steady state photoluminescence (PL) and the results are shown in Fig. 6b. The pristine perovskite film on glass substrate shows the highest PL intensity, indicating the strong charge recombination. As we deposited the perovskite films on the NIR-NiO_X and NIR-4 Co:NiO_X respectively, a significant PL quenching was observed because of the efficient charge transfer and hole extraction. Furthermore, the perovskite layer on the NIR-4 Co:NiO_X film exhibits the lower PL intensity than that of NIR-NiO_X, revealing the less charge recombination and charge accumulation. Concurrently, time-resolved photoluminescence (TRPL) measurements were performed as illustrated in Fig. 6c. The exponential decay profiles were fitted by the bi-exponential decay model as follow: $I(t) = A_1 \exp(-\frac{t}{\tau_1}) + A_2 \exp(-\frac{t}{\tau_2})$, where A_1 represents the fraction of charge transfer from perovskite to HTL, τ_1 represents the charge transfer lifetime, A_2 represents the fraction of charge recombination, and τ_2 is the charge recombination lifetime in perovskite layer. The average lifetime was calculated by following equation: $\tau_{avg} = \sum_i A_i\tau_i / \sum_i A_i$. All the parameters were summarized at Table 2. The decrease in the PL lifetime of NIR-4 Co:NiO_X/$MAPbI_3$ (41.1 ns) as compared to NIR-NiO_X/

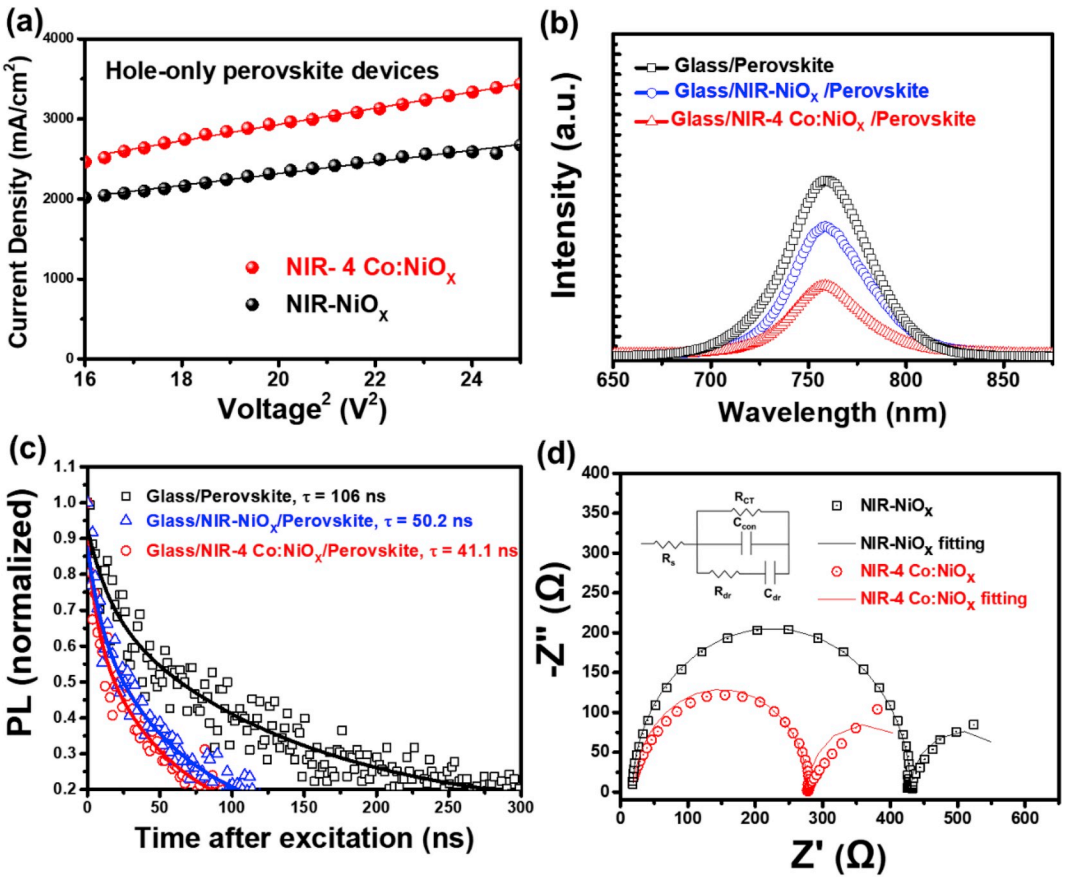

Fig. 6. **(a)** SCLC measurement for NIR-NiO_X and NIR-4 Co:NiO_X films. **(b)** PL spectra and **(c)** time-resolved PL spectra of perovskite films on pristine glass, NIR-NiO_X film and NIR-4 Co:NiO_X film. **(d)** Nyquist plots of PVSCs fabricated from NIR-NiO_X and NIR-4 Co:NiO_X films. The inset gives the equivalent circuit for fitting the Nyquist plots.

Table 2
Bi-exponential fitting results of PL decay for glass/perovskite, glass/NIR-NiO_X/perovskite, and glass/NIR-4 Co:NiO_X/perovskite.

Samples	A_1	τ_1 (ns)	A_2	τ_2 (ns)	$\tau_{average}$ (ns)
Glass/Perovskite	0.26	15.3	0.74	138	106
Glass/NIR-NiO_X/Peorvskite	0.25	9.14	0.75	63.6	50.2
Glass/NIR-4 Co:NiO_X/ Perovskite	0.30	6.91	0.70	55.8	41.1

$MAPbI_3$ (50.2 ns) and glass/$MAPbI_3$ (106 ns), indicating that the NIR-4 Co:NiO_X film has efficient hole extraction ability and thus suppresses the non-radiative recombination. These results can be attributed to the improved hole mobility of NIR-4 Co:NiO_X, well-matched work function level and enhanced built-in potential at the interface of perovskite/NIR-4 Co:NiO_X.

We further clarify the influencing factors to PCE improvement by using the impedance spectroscopy (EIS). The EIS measurement can provide the information of series resistance, interfacial resistance, recombination resistance and charge accumulation of PVSCs. Fig. 6d shows the Nyquist plots for devices fabricated from NIR-NiO_X and NIR-4 Co:NiO_X in the frequency range from 100 mHz to 1 MHz under 1 sun illumination at a bias of V_{oc}. Both Nyquist plots show the high and low frequency feature. Generally, the high frequency regime is related to charge transport resistance of the $MAPbI_3$/HTL interface whereas, the low frequency regime is considered to be attributed to a low frequency dielectric response of perovskite materials [55–57]. These two features can be fitted by the equivalent-circuit, comprising the series resistance, R_s, the interfacial charge transfer resistance, R_{CT}, the selective contact capacitance, C_{con}, the dielectric relaxation resistance, R_{dr}, and the dielectric contact capacitance, C_{dr}, as shown in the inset of Fig. 6d. The R_{CT} value obtained from the high frequency feature of devices fabricated from NIR-NiO_X and NIR-4 Co:NiO_X are 591.7±63.4 and 416.5±37.7 Ω, respectively, referring the lower charge transport resistance at the $MAPbI_3$/NIR-4 Co:NiO_X interface. The lower R_{CT} of the devices fabricated from NIR-4 Co:NiO_X films are attributed to the well-band alignment between $MAPbI_3$ and NIR-4 Co:NiO_X, resulting in a high built-in potential interface, as we mentioned in the UPS experiment. The high built-in potential can force a significant electron-hole separation, suppress the charge accumulation at $MAPbI_3$/NIR-4 Co:NiO_X interface, and thus reduce the R_{CT} value. As a result, we can conclude that the charge transport behavior at $MAPbI_3$/HTL interface dominates the improvement of devices performance for devices fabricated from NIR-4 Co:NiO_X.

In addition, we also demonstrate the stability of PVSCs fabricated from different HTLs, and the result are shown in Fig. 7. All the unencapsulated devices were stored in a nitrogen-filled glove box, and the performances of the devices were measured in ambient condition (25 °C and 40%~60% R.H.). Here, we use T_{80} lifetime, which is defined as the time over which the PCE decays to 80% of its initial value, to identify the stability of these devices. The T_{80} lifetimes of PVSCs fabricated from HP-NiO_X and NIR-NiO_X films are both around 200 h, however, the T_{80} lifetime of PVSCs fabricated from NIR-4 Co:NiO_X film is around 250 h. This result reveals that the PVSCs with NIR-4 Co:NiO_X HTL exhibits a better stability. According to previous literature reported [58], the charge accumulation at the interface between charge transport layer and perovskite layer would lead to the moisture-induced irreversible dissociation of perovskite, and thus lower the stability of PVSCs. Therefore, we believe that the improved stability of the PVSCs fabricated

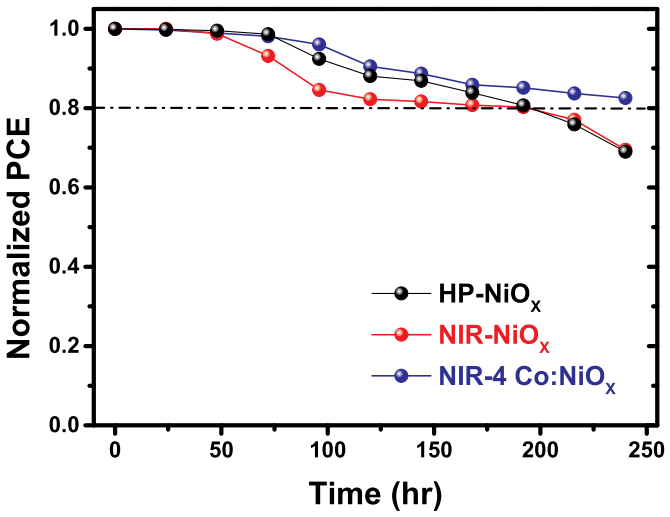

Fig. 7. Stability measurement of PVSCs fabricated from HP-NiO_X, NIR-NiO_X and NIR-4 Co:NiO_X films.

from NIR-4 Co:NiO_X is due to the suppression of charge accumulation at the interface between NIR-4 Co:NiO_X and perovskite layers.

4. Conclusion

In this study, we use the short wave NIR lamp at 2500 K as an alternative annealing source to conventional hot-plate to rapidly anneal sol-gel NiO_X films and systematically investigate the effect of NIR intensity on sol-gel NiO_X films. The XRD study reveals that the formation of crystalized NiO_X is accelerated by NIR exposure, while the morphologies of NIR-NiO_X and HP-NiO_X show no significant difference. Therefore, the PCE of PVSCs fabricated from NIR-NiO_X can maintain the same level as compare to that of HP-NiO_X. To further improve the PCE of PVSCs fabricated from NIR-NiO_X, we incorporate 4 mol% cobalt into NiO_X. The improvement of mobility, interface resistance and well-matched work function results in efficient hole extraction, less charge accumulation, and reducing V_{oc} loss. Thereby, the V_{oc}, J_{sc} and fill factor are significantly enhanced, and thus the PCE is improved from 15.99% to 17.77%. This study not only shows that the NIR radiation is a promising method for PVSCs to fulfill the requirements of low cost and low energy consumption large-scale production but also reveals the insight of Co dopant for high efficiency NiO_X based planar p-i-n PVSCs.

Author contribution

Pei-Huan Lee: Conceptualization, Methodology, Formal analysis, Investigation, Visualization, Writing – original draft. Bo-Ting Li: Validation, Formal analysis, Investigation. Chia-Feng Lee: Investigation. Zhi-Hao Huang: Investigation. Yu-Ching Huang: Writing – original draft, supervision. Wei-Fang Su: Writing – review editing, Project administration.

Declaration of competing interest

The authors declare that they have no known competing financial interests or personal relationships that could have appeared to influence the work reported in this paper.

Acknowledgements

Financial supports obtained from Ministry of Science and Technology of Taiwan (107-2218-E-131-007 and 108-3116-F-002-002-CC2) is highly appreciated.

Appendix A. Supplementary data

Supplementary data to this article can be found online at https://doi.org/10.1016/j.solmat.2019.110352.

References

[1] Y. Da, Y. Xuan, Q. Li, Quantifying energy losses in planar perovskite solar cells, Sol. Energy Mater. Sol. Cells 174 (2018) 206–213.
[2] T. Zhou, M. Wang, Z. Zang, L. Fang, Stable dynamics performance and high efficiency of ABX_3 -type super-alkali perovskites first obtained by introducing H_5O_2 cation, Adv. Energy Mater. 9 (2019) 1900664.
[3] T. Zhou, Y. Zhang, M. Wang, Z. Zang, X. Tang, Tunable electronic structures and high efficiency obtained by introducing superalkali and superhalogen into AMX_3-type perovskites, J. Power Sources 429 (2019) 120–126.
[4] T. Zhou, M. Wang, Z. Zang, X. Tang, L. Fang, Two-dimensional lead-free hybrid halide perovskite using superatom anions with tunable electronic properties, Sol. Energy Mater. Sol. Cells 191 (2019) 33–38.
[5] I. Cardinaletti, T. Vangerven, S. Nagels, R. Cornelissen, D. Schreurs, J. Hruby, J. Vodnik, D. Devisscher, J. Kesters, J. D'Haen, A. Franquet, V. Spampinato, T. Conard, W. Maes, W. Deferme, J.V. Manca, Organic and perovskite solar cells for space applications, Sol. Energy Mater. Sol. Cells 182 (2018) 121–127.
[6] National Renewable Energy Laboratory, Best Research-Cell Efficiencies. http://www.nrel.gov/pv/assets/images/efficiency_chart.jpg, 2019.
[7] L. Zhang, X. Liu, J. Li, S. McKechnie, Interactions between molecules and perovskites in halide perovskite solar cells, Sol. Energy Mater. Sol. Cells 175 (2018) 1–19.
[8] M. Wang, Z. Zang, B. Yang, X. Hu, K. Sun, L. Sun, Performance improvement of perovskite solar cells through enhanced hole extraction: the role of iodide concentration gradient, Sol. Energy Mater. Sol. Cells 185 (2018) 117–123.
[9] X. Zeng, T. Zhou, C. Leng, Z. Zang, M. Wang, W. Hu, X. Tang, S. Lu, L. Fang, M. Zhou, Performance improvement of perovskite solar cells by employing a CdSe quantum dot/PCBM composite as an electron transport layer, J. Mater. Chem. A 5 (2017) 17499–17505.
[10] J.P. Correa Baena, L. Steier, W. Tress, M. Saliba, S. Neutzner, T. Matsui, F. Giordano, T.J. Jacobsson, A.R. Srimath Kandada, S.M. Zakeeruddin, A. Petrozza, A. Abate, M.K. Nazeeruddin, M. Grätzel, A. Hagfeldt, Highly efficient planar perovskite solar cells through band alignment engineering, Energy Environ. Sci. 8 (2015) 2928–2934.
[11] A. Guerrero, G. Garcia-Belmonte, I. Mora-Sero, J. Bisquert, Y.S. Kang, T. J. Jacobsson, J.-P. Correa-Baena, A. Hagfeldt, Properties of contact and bulk impedances in hybrid lead halide perovskite solar cells including inductive loop elements, J. Phys. Chem. C 120 (2016) 8023–8032.
[12] J.Y. Jeng, K.C. Chen, T.Y. Chiang, P.Y. Lin, T.D. Tsai, Y.C. Chang, T.F. Guo, P. Chen, T.C. Wen, Y.J. Hsu, Nickel oxide electrode interlayer in $CH_3NH_3PbI_3$ perovskite/PCBM planar-heterojunction hybrid solar cells, Adv. Mater. 26 (2014) 4107–4113.
[13] H. Zhou, Q. Chen, G. Li, S. Luo, T.-b. Song, H.-S. Duan, Z. Hong, J. You, Y. Liu, Y. Yang, Interface engineering of highly efficient perovskite solar cells, Science 345 (2014) 542–546.
[14] L. Hu, M. Li, K. Yang, Z. Xiong, B. Yang, M. Wang, X. Tang, Z. Zang, X. Liu, B. Li, Z. Xiao, S. Lu, H. Gong, J. Ouyang, K. Sun, PEDOT:PSS monolayers to enhance the hole extraction and stability of perovskite solar cells, J. Mater. Chem. A 6 (2018) 16583–16589.
[15] J.C. Yu, J.A. Hong, E.D. Jung, D.B. Kim, S.M. Baek, S. Lee, S. Cho, S.S. Park, K. J. Choi, M.H. Song, Highly efficient and stable inverted perovskite solar cell employing PEDOT:GO composite layer as a hole transport layer, Sci. Rep. 8 (2018) 1070.
[16] G. Adam, M. Kaltenbrunner, E.D. Głowacki, D.H. Apaydin, M.S. White, H. Heilbrunner, S. Tombe, P. Stadler, B. Ernecker, C.W. Klampfl, N.S. Sariciftci, M. C. Scharber, Solution processed perovskite solar cells using highly conductive PEDOT:PSS interfacial layer, Sol. Energy Mater. Sol. Cells 157 (2016) 318–325.
[17] Y. Liu, Z. Liu, E.-C. Lee, High-performance inverted perovskite solar cells using doped poly(triarylamine) as the hole transport layer, ACS Appl. Energy Mater. 2 (2019) 1932–1942.
[18] C. Xu, Z. Liu, E.-C. Lee, High-performance metal oxide-free inverted perovskite solar cells using poly(bis(4-phenyl)(2,4,6-trimethylphenyl)amine) as the hole transport layer, J. Mater. Chem. C 6 (2018) 6975–6981.
[19] J. Kim, N. Park, J.S. Yun, S. Huang, M.A. Green, A.W.Y. Ho-Baillie, An effective method of predicting perovskite solar cell lifetime–Case study on planar $CH_3NH_3PbI_3$ and $HC(NH_2)_2PbI_3$ perovskite solar cells and hole transfer materials of spiro-OMeTAD and PTAA, Sol. Energy Mater. Sol. Cells 162 (2017) 41–46.
[20] B.-S. Kim, T.-M. Kim, M.-S. Choi, H.-S. Shim, J.-J. Kim, Fully vacuum–processed perovskite solar cells with high open circuit voltage using MoO_3/NPB as hole extraction layers, Org. Electron. 17 (2015) 102–106.
[21] N. Wijeyasinghe, A. Regoutz, F. Eisner, T. Du, L. Tsetseris, Y.-H. Lin, H. Faber, P. Pattanasattayavong, J. Li, F. Yan, M.A. McLachlan, D.J. Payne, M. Heeney, T. D. Anthopoulos, copper(I) thiocyanate (CuSCN) hole-transport layers processed from aqueous precursor solutions and their application in thin-film transistors and highly efficient organic and organometal halide perovskite solar cells, Adv. Funct. Mater. 27 (2017) 1701818.
[22] K. Zhao, R. Munir, B. Yan, Y. Yang, T. Kim, A. Amassian, Solution-processed inorganic copper(i) thiocyanate (CuSCN) hole transporting layers for efficient p–i–n perovskite solar cells, J. Mater. Chem. A 3 (2015) 20554–20559.

[23] T.H. Chowdhury, M. Akhtaruzzaman, M.E. Kayesh, R. Kaneko, T. Noda, J.-J. Lee, A. Islam, Low temperature processed inverted planar perovskite solar cells by r-GO/CuSCN hole-transport bilayer with improved stability, Sol. Energy 171 (2018) 652–657.

[24] G. Murugadoss, R. Thangamuthu, S.M. Senthil Kumar, Fabrication of $CH_3NH_3PbI_3$ perovskite-based solar cells: developing various new solvents for CuSCN hole transport material, Sol. Energy Mater. Sol. Cells 164 (2017) 56–62.

[25] Z.-K. Yu, W.-F. Fu, W.-Q. Liu, Z.-Q. Zhang, Y.-J. Liu, J.-L. Yan, T. Ye, W.-T. Yang, H.-Y. Li, H.-Z. Chen, Solution-processed CuO as an efficient hole-extraction layer for inverted planar heterojunction perovskite solar cells, Chin. Chem. Lett. 28 (2017) 13–18.

[26] W. Sun, Y. Li, S. Ye, H. Rao, W. Yan, H. Peng, Y. Li, Z. Liu, S. Wang, Z. Chen, L. Xiao, Z. Bian, C. Huang, High-performance inverted planar heterojunction perovskite solar cells based on a solution-processed CuOx hole transport layer, Nanoscale 8 (2016) 10806–10813.

[27] M. Najafi, F. Di Giacomo, D. Zhang, S. Shanmugam, A. Senes, W. Verhees, A. Hadipour, Y. Galagan, T. Aernouts, S. Veenstra, R. Andriessen, Highly efficient and stable flexible perovskite solar cells with metal oxides nanoparticle charge extraction layers, Small 14 (2018) 1702775.

[28] J. Tang, D. Jiao, L. Zhang, X. Zhang, X. Xu, C. Yao, J. Wu, Z. Lan, High-performance inverted planar perovskite solar cells based on efficient hole-transporting layers from well-crystalline NiO nanocrystals, Sol. Energy 161 (2018) 100–108.

[29] W. Chen, Y. Wu, Y. Yue, J. Liu, W. Zhang, X. Yang, H. Chen, E. Bi, I. Ashraful, M. Grätzel, L. Han, Efficient and stable large-area perovskite solar cells with inorganic charge extraction layers, Science 350 (2015) 944–948.

[30] J.H. Kim, P.W. Liang, S.T. Williams, N. Cho, C.C. Chueh, M.S. Glaz, D.S. Ginger, A. K. Jen, High-performance and environmentally stable planar heterojunction perovskite solar cells based on a solution-processed copper-doped nickel oxide hole-transporting layer, Adv. Mater. 27 (2015) 695–701.

[31] W. Chen, Y. Wu, J. Fan, A.B. Djurišić, F. Liu, H.W. Tam, A. Ng, C. Surya, W.K. Chan, D. Wang, Z.-B. He, Understanding the doping Effect on NiO: toward high-performance inverted perovskite solar cells, Adv. Energy Mater. 8 (2018) 1703519.

[32] Q. He, K. Yao, X. Wang, X. Xia, S. Leng, F. Li, Room-temperature and solution-processable Cu-doped nickel oxide nanoparticles for efficient hole-transport layers of flexible large-area perovskite solar cells, ACS Appl. Mater. Interfaces 9 (2017) 41887–41897.

[33] H.-S. Kim, J.-Y. Seo, H. Xie, M. Lira-Cantu, S.M. Zakeeruddin, M. Grätzel, A. Hagfeldt, Effect of Cs-incorporated NiOx on the performance of perovskite solar cells, ACS Omega 2 (2017) 9074–9079.

[34] W. Chen, F.-Z. Liu, X.-Y. Feng, A.B. Djurišić, W.K. Chan, Z.-B. He, Cesium doped NiOx as an efficient hole extraction layer for inverted planar perovskite solar cells, Adv. Energy Mater. 7 (2017) 1700722.

[35] A.B. Huang, J.T. Zhu, J.Y. Zheng, Y. Yu, Y. Liu, S.W. Yang, S.H. Bao, L. Lei, P. Jin, Achieving high-performance planar perovskite solar cells with co-sputtered Co-doping NiOx hole transport layers by efficient extraction and enhanced mobility, J. Mater. Chem. C 4 (2016) 10839–10846.

[36] Y. Xie, K. Lu, J. Duan, Y. Jiang, L. Hu, T. Liu, Y. Zhou, B. Hu, Enhancing photovoltaic performance of inverted planar perovskite solar cells by cobalt-doped nickel oxide hole transport layer, ACS Appl. Mater. Interfaces 10 (2018) 14153–14159.

[37] J. Zheng, L. Hu, J.S. Yun, M. Zhang, C.F.J. Lau, J. Bing, X. Deng, Q. Ma, Y. Cho, W. Fu, C. Chen, M.A. Green, S. Huang, A.W.Y. Ho-Baillie, Solution-processed, silver-doped NiOx as hole transporting layer for high-efficiency inverted perovskite solar cells, ACS Appl. Energy Mater. 1 (2018) 561–570.

[38] J. Zhang, W. Mao, X. Hou, J. Duan, J. Zhou, S. Huang, W. Ou-Yang, X. Zhang, Z. Sun, X. Chen, Solution-processed Sr-doped NiOx as hole transport layer for efficient and stable perovskite solar cells, Sol. Energy 174 (2018) 1133–1141.

[39] J. Cui, F. Meng, H. Zhang, K. Cao, H. Yuan, Y. Cheng, F. Huang, M. Wang, $CH_3NH_3PbI_3$-based planar solar cells with magnetron-sputtered nickel oxide, ACS Appl. Mater. Interfaces 6 (2014) 22862–22870.

[40] K.C. Wang, P.S. Shen, M.H. Li, S. Chen, M.W. Lin, P. Chen, T.F. Guo, Low-temperature sputtered nickel oxide compact thin film as effective electron blocking layer for mesoscopic $NiO/CH_3NH_3PbI_3$ perovskite heterojunction solar cells, ACS Appl. Mater. Interfaces 6 (2014) 11851–11858.

[41] S. Seo, I.J. Park, M. Kim, S. Lee, C. Bae, H.S. Jung, N.G. Park, J.Y. Kim, H. Shin, An ultra-thin, un-doped NiO hole transporting layer of highly efficient (16.4%) organic-inorganic hybrid perovskite solar cells, Nanoscale 8 (2016) 11403–11412.

[42] J.W. Jung, C.C. Chueh, A.K. Jen, A Low-Temperature, Solution-processable, Cu-doped nickel oxide hole-transporting layer via the combustion method for high-performance thin-film perovskite solar cells, Adv. Mater. 27 (2015) 7874–7880.

[43] Z. Liu, J. Chang, Z. Lin, L. Zhou, Z. Yang, D. Chen, C. Zhang, S.F. Liu, Y. Hao, High-performance planar perovskite solar cells using low temperature, solution-combustion-based nickel oxide hole transporting layer with efficiency exceeding 20%, Adv. Energy Mater. 8 (2018) 1703432.

[44] M.-H. Jao, C.-C. Cheng, C.-F. Lu, K.-C. Hsiao, W.-F. Su, Low temperature and rapid formation of high quality metal oxide thin film via a hydroxide-assisted energy conservation strategy, J. Mater. Chem. C 6 (2018) 9941–9949.

[45] K. Hooper, M. Carnie, C. Charbonneau, T. Watson, Near infrared radiation as a rapid heating technique for TiO_2 films on glass mounted dye-sensitized solar cells, Int. J. Photoenergy 2014 (2014) 1–8.

[46] J. Baker, K. Hooper, S. Meroni, A. Pockett, J. McGettrick, Z. Wei, R. Escalante, G. Oskam, M. Carnie, T. Watson, High throughput fabrication of mesoporous carbon perovskite solar cells, J. Mater. Chem. A 5 (2017) 18643–18650.

[47] J. Troughton, C. Charbonneau, M.J. Carnie, M.L. Davies, D.A. Worsley, T. M. Watson, Rapid processing of perovskite solar cells in under 2.5 seconds, J. Mater. Chem. A 3 (2015) 9123–9127.

[48] V.L. Pool, B. Dou, D.G. Van Campen, T.R. Klein-Stockert, F.S. Barnes, S.E. Shaheen, M.I. Ahmad, M.F. van Hest, M.F. Toney, Thermal engineering of $FAPbI_3$ perovskite material via radiative thermal annealing and in situ XRD, Nat. Commun. 8 (2017) 14075.

[49] Y.-C. Huang, C.-F. Li, Z.-H. Huang, P.-H. Liu, C.-S. Tsao, Rapid and sheet-to-sheet slot-die coating manufacture of highly efficient perovskite solar cells processed under ambient air, Sol. Energy 177 (2019) 255–261.

[50] B. Sharma, S. Singh, S. Pareek, A. Agasti, S. Mallick, D. Kabra, P. Bhargava, Radiative and conductive thermal annealing of hybrid organic-inorganic perovskite layer, Sol. Energy Mater. Sol. Cells 195 (2019) 353–357.

[51] Z. Qiu, H. Gong, G. Zheng, S. Yuan, H. Zhang, X. Zhu, H. Zhou, B. Cao, Enhanced physical properties of pulsed laser deposited NiO films via annealing and lithium doping for improving perovskite solar cell efficiency, J. Mater. Chem. C 5 (2017) 7084–7094.

[52] E. Antolini, Sintering of $Li_xNi_{1-x}O$ solid solutions at 1200 ^oC, J. Mater. Sci. 27 (1992) 3335.

[53] S. Nandy, B. Saha, M.K. Mitra, K.K. Chattopadhyay, Effect of oxygen partial pressure on the electrical and optical properties of highly (200) oriented p-type Ni1–xO films by DC sputtering, J. Mater. Sci. 42 (2007) 5766–5772.

[54] W.-L. Jang, Y.-M. Lu, W.-S. Hwang, W.-C. Chen, Electrical properties of Li-doped NiO films, J. Eur. Ceram. Soc. 30 (2010) 503–508.

[55] G.A. Sepalage, S. Meyer, A. Pascoe, A.D. Scully, F. Huang, U. Bach, Y.-B. Cheng, L. Spiccia, Copper(I) iodide as hole-conductor in planar perovskite solar cells: probing the origin of J-V hysteresis, Adv. Funct. Mater. 25 (2015) 5650–5661.

[56] C. Eames, J.M. Frost, P.R. Barnes, B.C. O'Regan, A. Walsh, M.S. Islam, Ionic transport in hybrid lead iodide perovskite solar cells, Nat. Commun. 6 (2015) 7497.

[57] V. Gonzalez-Pedro, E.J. Juarez-Perez, W.S. Arsyad, E.M. Barea, F. Fabregat-Santiago, I. Mora-Sero, J. Bisquert, General working principles of $CH_3NH_3PbX_3$ perovskite solar cells, Nano Lett. 14 (2014) 888–893.

[58] N. Ahn, K. Kwak, M.S. Jang, H. Yoon, B.Y. Lee, J.-K. Lee1, P.V. Pikhitsa, J. Byun, M. Cho, Trapped charge-driven degradation of perovskite solar cells, Nat. Commun. 7 (2016) 13422.